

Supplementary Information

Synthesis of Large and Few Atomic Layers of Hexagonal Boron Nitride on Melted Copper

Majharul Haque Khan¹, Zhenguo Huang^{1,*}, Feng Xiao¹, Gilberto Casillas², Zhixin Chen³, Paul J. Molino⁴ & Hua Kun Liu¹

¹Institute for Superconducting and Electronic Materials, ²Electron Microscopy Center, ³Bluescope Steel Metallurgical Center, ⁴Intelligent Polymer Research Institute, University of Wollongong, Wollongong, NSW 2500, Australia.

Corresponding author: zhenguo@uow.edu.au

1. Thermal decomposition of ammonia borane

Ammonia borane is decomposed at 110°C, and this leads to the formation of borazine ($B_3N_3H_6$), hydrogen, polyaminoborhane $[(BH_2NH_2)_n]$, polyiminoborane $[(BHNH)_n]$, polyborazylene $[(B_3N_3H_6)_n]$, diborane (B_2H_6), and ammonia (NH_3) ¹⁻⁵. Among these, polymeric compounds have been reported to degrade the quality of *h*-BNNS^{6,7}. In this study, ammonia borane was

decomposed outside the CVD furnace in a Schlenk reaction tube fitted with a glass filter that prevents these polymeric compounds from entering the reaction zone. Therefore, the volatiles reaching the substrate are H₂ and borazine, since trace amounts of B₂H₆ and NH₃ will form solid amine complexes inside the tubing before reaching the substrate⁸. ~~Borazine tends to polymerize into solid polyborazylene at room temperature, so it requires low temperature for long-term storage. It reacts with moisture to form boric acid, ammonia, and hydrogen^{2,6}. It is also toxic.~~ The thermal decomposition of ammonia borane in this experiment serves as the *in-situ* source of borazine. The decomposition products of ammonia borane were carried into the reaction zone by a gas flow of 100 sccm 10% H₂ in Ar through the Schlenk reaction tube.

2. Results and discussion

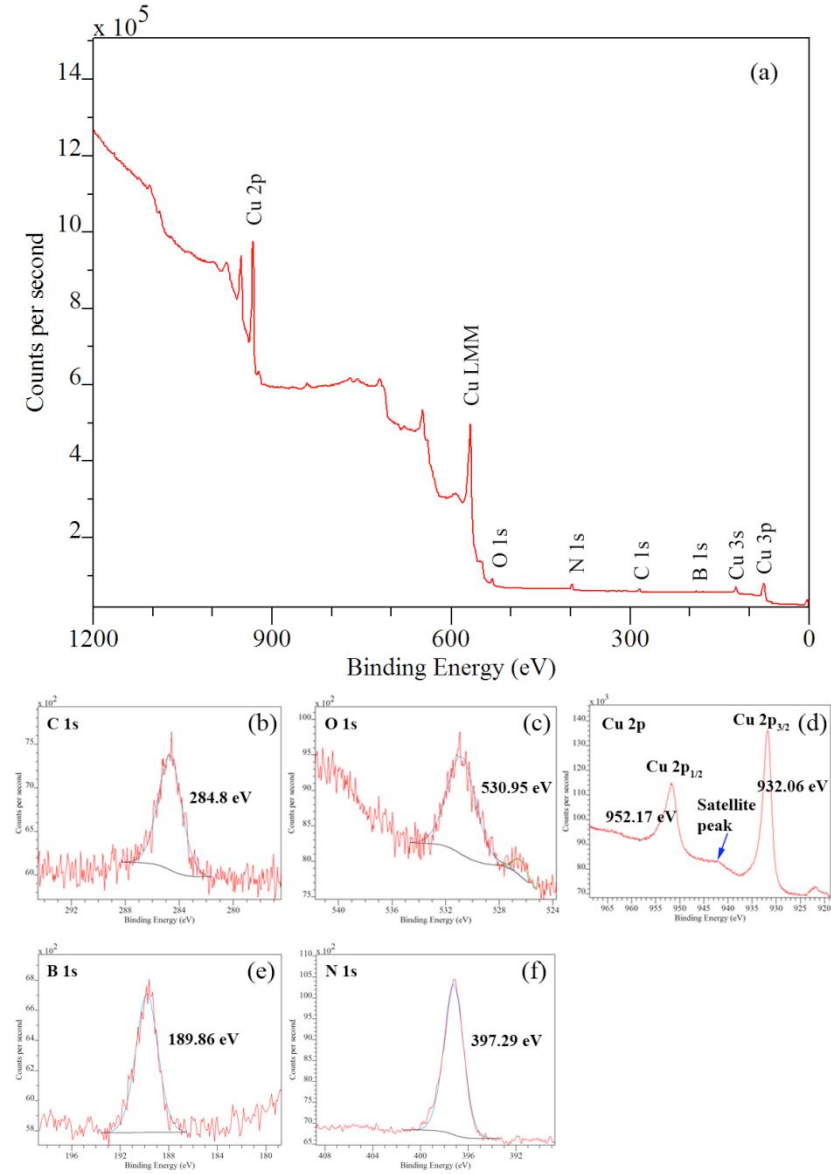


Figure S1: (a) Representative XPS survey spectrum of *h*-BNNS. The small C 1s (b) and O 1s (c) peaks might have come from surface contamination by air in between the synthesis and the XPS measurements. The C 1s and O 1s peaks were also observed in a blank annealed copper sample. From the integrated peak area analysis of B 1s (e) and N 1s (f), a nearly 1:1 B/N atomic ratio is obtained, indicating sp^2 *h*-BN formation. The Shirley background function was used for B 1s and

N 1s peak background correction, and a 70% Gaussian, 30% Lorentzian combined function was used for peak-fitting analysis.

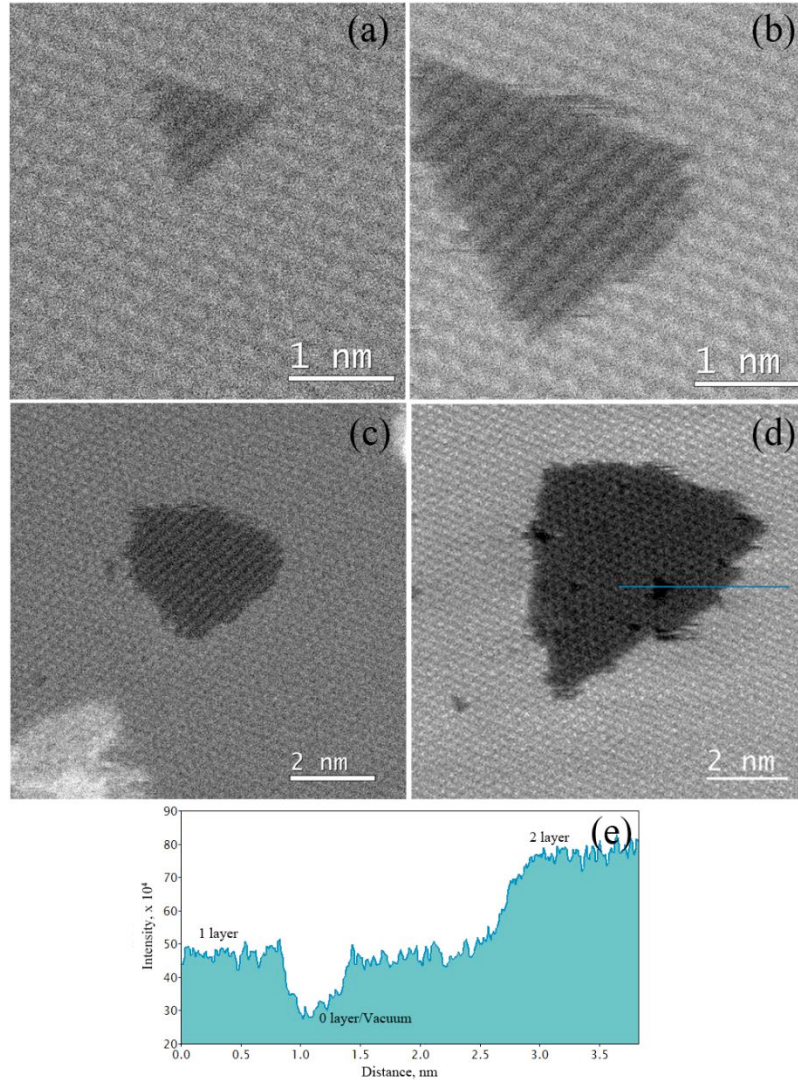


Figure S2: Electron knock-on damage and layer opening in bi-layer *h*-BNNS, observed in ADF-STEM imaging mode at 80 kV: (a-d) Both B and N atoms were gradually knocked out of the top layer under electron beam irradiation, forming a triangle. This geometry is probably associated with the more energetically favorable nitrogen edge termination in *h*-BN^{9,10}. The low operation voltage (80 kV) is below the critical knock-on energy of nitrogen of 84 kV, however, both B and

N have been found to be knocked out of the second layer. It can be deduced that B monovacancy defects were formed initially due to its lower knock-on energy of 74 kV, and consequently, both B and N atoms can be removed below their critical knock-on energy due to the presence of these defects¹¹. B monovacancy creation by electron beam has also been reported at higher operating voltage (120 kV)⁹. HAADF-STEM imaging can be an important tool to identify elements and the atomic layer thickness, by taking advantage of the Z contrast¹². Direct layer identification from the intensity line profile analysis across the HAADF-STEM image in (d) clearly shows the vacancies, and the mono-layer and bi-layer *h*-BNNS regions. Figure (d) was smoothed to lower the background noise in the line profile image (e).

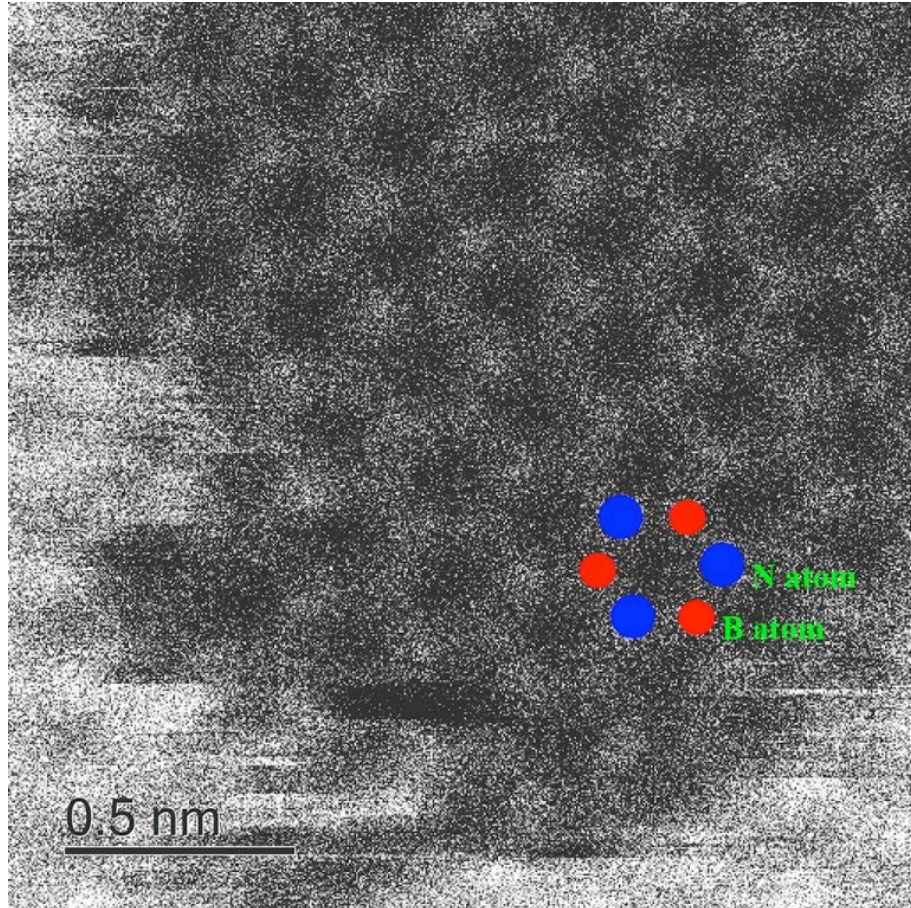


Figure S3: Raw HAADF-STEM image from a mono-layer *h*-BNNS region. The heavier N atoms are slightly brighter than the B atoms. B and N atoms have been tagged with red and blue circles, respectively.

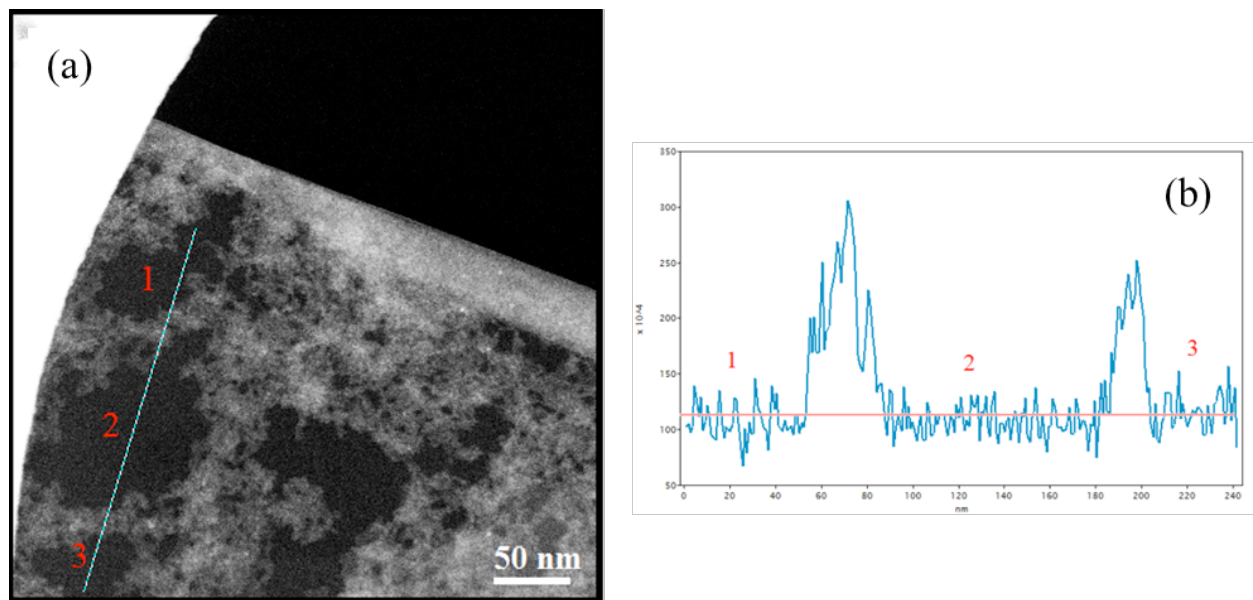


Figure S4: (a) HAADF-STEM image of *h*-BNNS grown on melted copper and (b) intensity profile along the line in (a). Similar intensity in the three zones indicates homogeneous *h*-BNNS in that region. The relatively bright regions are the PMMA residues.

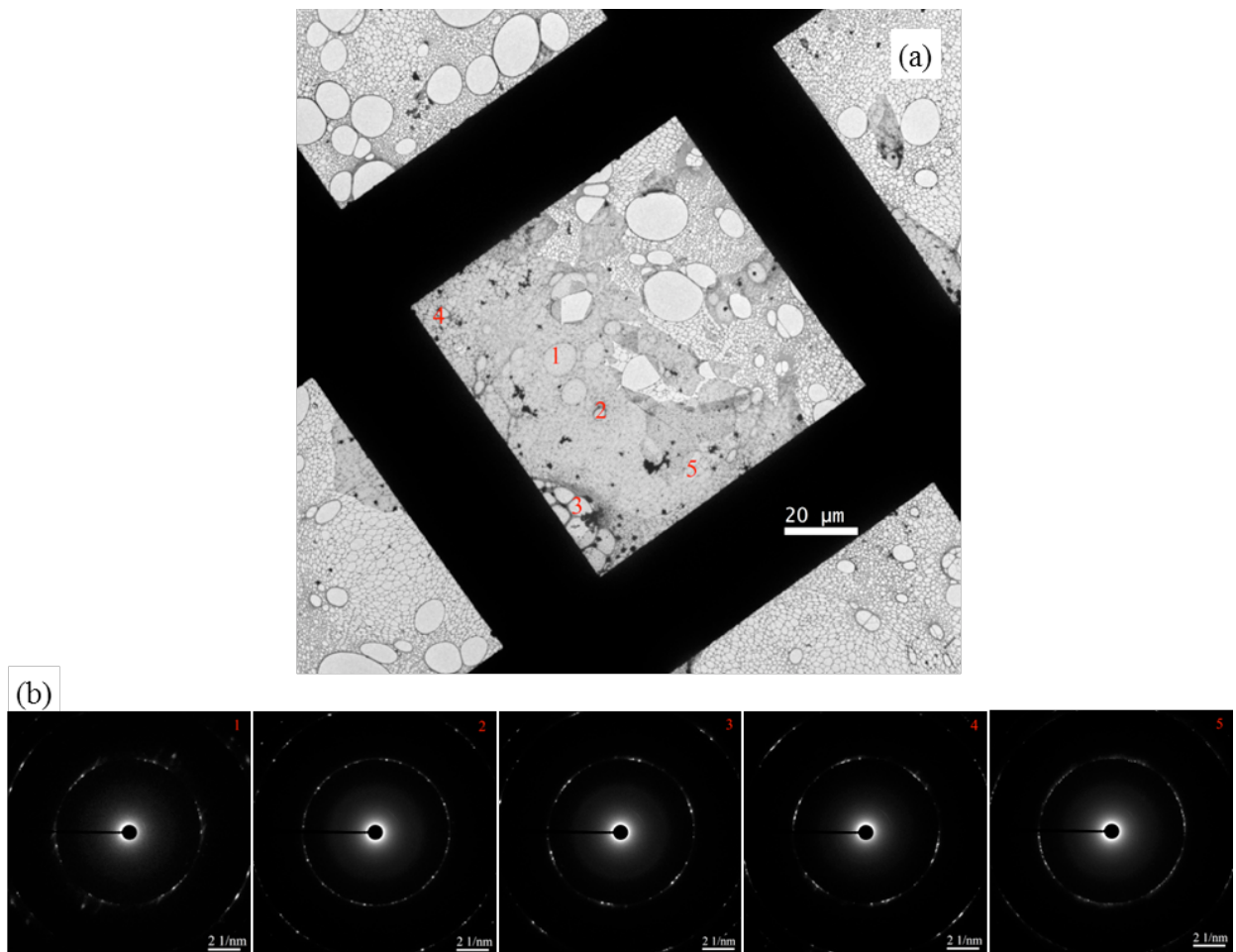


Figure S5: (a) Low magnification TEM image of transferred *h*-BNNS grown on solid copper. (b) SAED patterns obtained from the five areas marked in (a) show the polycrystalline nature of the *h*-BNNS.

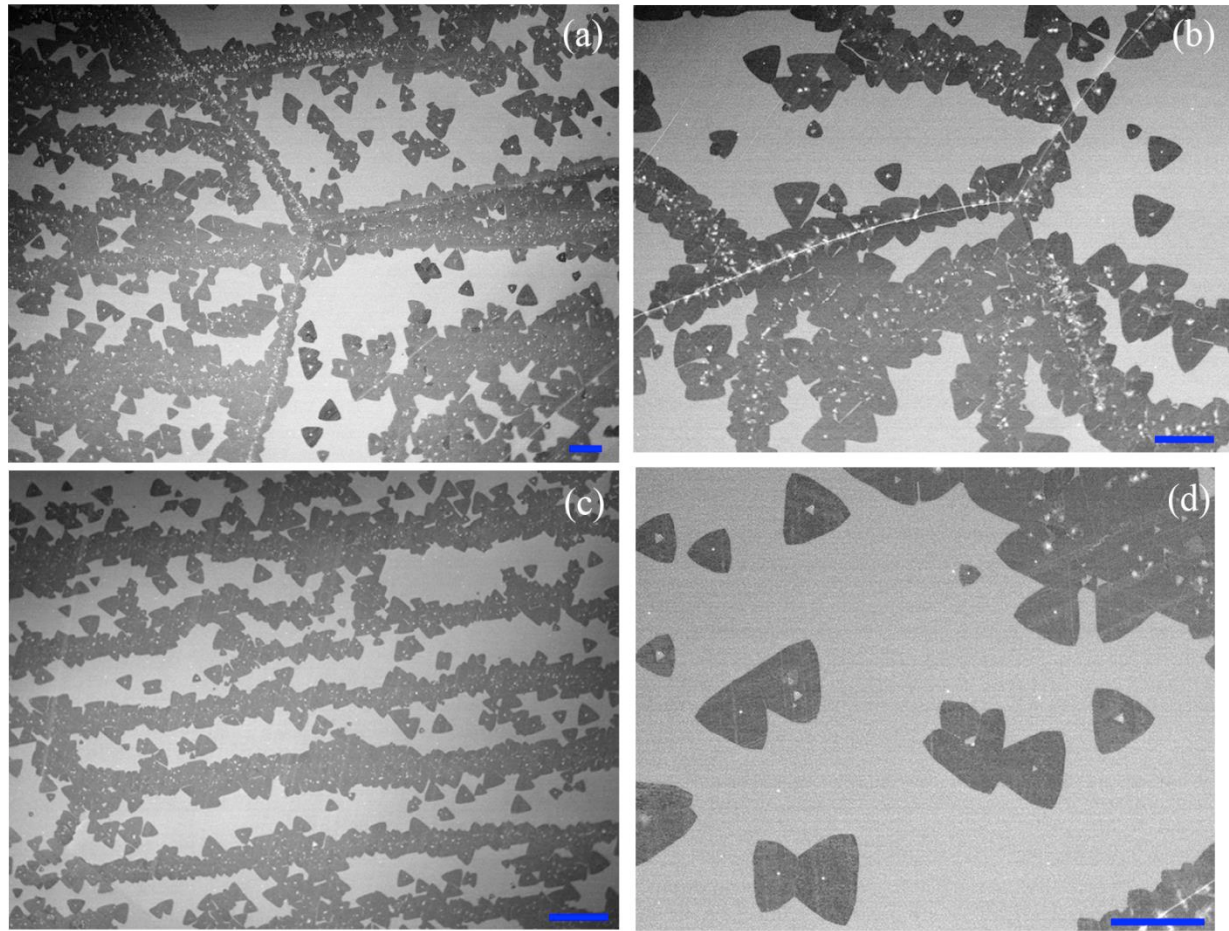


Figure S6: Initial growth of *h*-BNNS on solid copper. (a-c) *h*-BN triangular domains, mostly isolated and around 4 μm in size, preferentially grow along the grain boundaries and defect lines. At the center of each domain, small adlayers can be observed. (d) Coalescence of individual triangular domains. The scale bar is 5 μm in all the images.

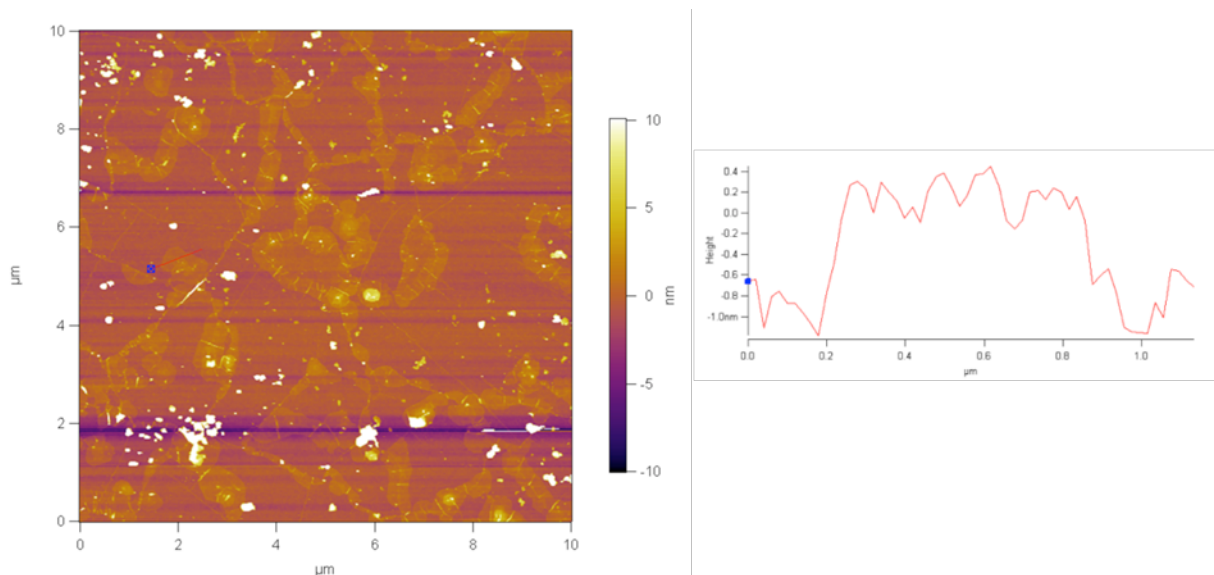


Figure S7: Discontinuous and inhomogeneous *h*-BNNS grown on solid copper with a 200 sccm 10% H₂/Ar carrier gas flow. The corresponding line profile shows fragmented 1 nm thick *h*-BNNS.

References

- S1. Frueh, S.. Kellett, R., Mallory, C. *et al.* Pyrolytic decomposition of ammonia borane to boron nitride. *Inorganic Chemistry* **50**, 783–92 (2011).
- S2. Wolf, G., Baumann, J., Baitalow, F. & Hoffmann, F. P. Calorimetric process monitoring of thermal decomposition. *Thermochimica Acta* **343**, 19–25 (2000).
- S3. Baitalow, F., Baumann, J., Wolf, G., Jaenicke-Rößler, K. & Leitner, G. Thermal decomposition of B–N–H compounds investigated by using combined thermoanalytical methods. *Thermochimica Acta* **391**, 159–168 (2002).
- S4. Li, J., Bernard, S., Salles, V., Gervais, C., Miele, P. Preparation of Polyborazylene-Derived Bulk Boron Nitride with Tunable Properties by Warm-Pressing and Pressureless Pyrolysis. *Chemistry of Materials* **22**, 2920–2929 (2010).
- S5. Whittell, G. R. & Manners, I. Advances with ammonia-borane: Improved recycling and use as a precursor to atomically thin BN films. *Angewandte Chemie (International Edition in English)* **50**, 10288–9 (2011).

- S6. Kim, K. K., Hsu, A., Jia, X. *et al.* Synthesis of monolayer hexagonal boron nitride on Cu foil using chemical vapor deposition. *Nano Letters* **12**, 161–166 (2012).
- S7. Lee, K. H., Shin, H., Lee, J. *et al.* Large-scale synthesis of high-quality hexagonal boron nitride nanosheets for large-area graphene electronics. *Nano Letters* **12**, 714–8 (2012).
- S8. Gomez-Aleixandre, C., Diaz, D., Orgaz, F. & Albella, J. M. Reaction of diborane and ammonia gas mixtures in a chemical vapor deposition hot-wall reactor. *The Journal of Physical Chemistry* **97**, 11043–11046 (1993).
- S9. Jin, C., Lin, F., Suenaga, K. & Iijima, S. Fabrication of a Freestanding Boron Nitride Single Layer and Its Defect Assignments. *Physical Review Letters* **102**, 195505 (2009).
- S10. Liu, Y., Bhowmick, S. & Yakobson, B. I. BN white graphene with “colorful” edges: the energies and morphology. *Nano Letters* **11**, 3113–6 (2011).
- S11. Zobelli, A., Gloter, A., Ewels, C., Seifert, G. & Collieux, C. Electron knock-on cross-section of carbon and boron nitride nanotubes. *Physical Review B* **75**, 245402 (2007).
- S12. Liu, Z., Gong Y., Zhou, W. *et al.* Ultrathin high-temperature oxidation-resistant coatings of hexagonal boron nitride. *Nature Communications* **4**, 2541 (2013).